Dynamics of individual molecules of linear polyethylene liquids under shear: Atomistic simulation and comparison with a free-draining bead-rod chain

J. M. Kim, B. J. Edwards,[a] D. J. Keffer, and B. Khomami

Department of Chemical and Biomolecular Engineering, University of Tennessee, Knoxville, Tennessee 37996

(Received 5 July 2009; final revision received 22 December 2009; published 19 February 2010)

Synopsis

Nonequilibrium molecular dynamics (NEMD) simulations of a dense liquid composed of linear polyethylene chains were performed to investigate the chain dynamics under shear. Brownian dynamics (BD) simulations of a freely jointed chain with equivalent contour length were also performed in the case of a dilute solution. This allowed for a close comparison of the chain dynamics of similar molecules for two very different types of liquids. Both simulations exhibited a distribution of the end-to-end vector, $|\mathbf{R}_{ete}|$, with Gaussian behavior at low Weissenberg number (Wi). At high Wi, the NEMD distribution was bimodal, with two peaks associated with rotation and stretching of the individual molecules. BD simulations of a dilute solution did not display a bimodal character; distributions of $|\mathbf{R}_{ete}|$ ranged from tightly coiled to fully stretched configurations. The simulations revealed a tumbling behavior of the chains and correlations between the components of $\mathbf{R}_{ete}$ exhibited characteristic frequencies of tumbling, which scaled as $Wi^{-0.75}$. Furthermore, after a critical Wi of approximately 2, another characteristic time scale appeared which scaled as $Wi^{-0.63}$. Although the free-draining solution is very different than the dense liquid, the BD simulations revealed a similar behavior, with the characteristic time scales mentioned above scaling as $Wi^{-0.68}$ and $Wi^{-0.66}$. © *2010 The Society of Rheology.* [DOI: 10.1122/1.3314298]

I. INTRODUCTION

Observations of the motions of individual chain molecules are crucial to further development and refinement of rheological and topological models of the dynamics of polymeric liquids. Most past modeling efforts have been aimed at the description of the evolution of bulk-averaged quantities, such as the conformation or stress tensors, under the influence of an applied external flow field [Bird *et al.* (1987a, 1987b)]. These preaveraged theories are applicable to chain liquids at low field strength, but their descriptions of the rheological behavior tend to break down once the field strength drives the fluid beyond the linear viscoelastic regime. For example, simple kinetic theories of dilute Hookean dumbbell solutions are generally rendered computationally efficient by preaveraging the diffusion equation for the distribution of the dumbbell connector vector over the entire configuration space. This is accomplished by defining the conformation

[a]Author to whom correspondence should be addressed; electronic mail: bje@utk.edu

tensor, mentioned above, as the second moment of the configurational distribution function [Bird *et al.* (1987b)]. Unfortunately, this procedure implies a substantial degree of coarse-graining of the degrees of freedom, resulting in characteristic evolution equations for variables (again, such as the conformation tensor or the extra stress tensor) which change on macroscopic length and time scales. Consequently, any information that is present on microscopic time scales is effectively removed from the final evolution equations that describe the dynamical response of the chain liquid. This readily explains why these pre-averaged theories break down in the nonlinear viscoelastic regime where the time scales of the flow can become smaller than those associated with the time evolution of the macroscopic variables. (Recall that as strain rate is increased, its reciprocal, associated with the characteristic time scale of the flow, decreases.) Many examples of the failure of pre-averaged models, especially at high strain rates, were discussed by Larson (1988).

Many attempts have been made to extend the validity of rheological equations of state into the nonlinear viscoelastic regime, such as network theories [Bird *et al.* (1987b)] and reptation-based modeling [Doi and Edwards (1986)]. In the reptation-based model of Doi and Edwards (1986), a generic chain is assumed to undergo snake-like motion within a contorted tube formed by neighboring chains. Consequently, motion along the chain contour is much less restrained than motion perpendicular to it. A characteristic time scale is assigned to this motion, τ_D, which is called the "reptation" or "disengagement" time scale; conceptually, this is the time required for the chain to disengage from its original tube [Doi and Edwards (1986)]. This time scale is generally some multiple of the fluid's Rouse time, τ_R, under conditions of equilibrium.

Although the most comprehensive versions of reptation-based theories perform well at low shear rates ($\dot{\gamma} < 1/\tau_D$) [Larson (1999)] and have recently attained success at intermediate shear rates ($1/\tau_D < \dot{\gamma} < 1/\tau_R$) [Mhetar and Archer (2000); Islam *et al.* (2003)], they still fail to describe the rheology of entangled polymeric liquids at high shear rates where the associated time scales become relatively small ($1/\tau_R < \dot{\gamma}$) [Teixeira *et al.* (2007)].

Until recently, light scattering and birefringence experiments were used for analyzing the orientational and configurational changes of polymer chains undergoing flow. However, these types of experimentation were unable to track configurational changes of individual polymer chains. Consequently, these measurement techniques were restricted to examining bulk fluid properties and could not distinguish between phenomena that occur over disparate time scales; however, this does not mean that the dynamics of individual chain molecules do not affect the observed birefringence and light scattering patterns. Indeed, as discussed below and by Kim *et al.* (2009), the tumbling motion of individual chain molecules at high shear rates might be responsible for the breakdown under shear of the stress-optical rule in many polymeric liquids.

Relatively recent direct visualization of individual polymer chains using video microscopy offers the possibility to explore the motions of individual chain molecules undergoing flow [Teixeira *et al.* (2005, 2007); Smith and Chu (1998); Smith *et al.* (1999); LeDuc *et al.* (1999); Schroeder *et al.* (2005); Robertson and Smith (2007)]. These initial studies have seriously called into question many of the assumptions used to model polymer flow dynamics. Smith *et al.* (1999) and LeDuc *et al.* (1999) simultaneously examined dilute solutions of DNA, in which the dynamics of individual, labeled chains were visualized under shear in the flow-vorticity plane using video microscopy. These results demonstrated that the flexible polymer chains experienced both deformation and tumbling under shear, as a function of the Weissenberg number ($Wi = \tau_R \dot{\gamma}$). Schroeder *et al.* (2005) and Teixeira *et al.* (2005, 2007) visualized and tracked individual configurational

changes of fluorescently labeled DNA solutions under steady shear flow in the flow-gradient plane for concentrations ranging from dilute to highly entangled. These experiments again demonstrated the tumbling and stretching dynamics of individual chains, which depended on both *Wi* and concentration, but the evidence was more direct since the visualization was carried out in the flow-gradient plane. They also demonstrated a clear *quasi-periodic* tumbling of the individual DNA molecules in dilute solution at high *Wi*, with a characteristic frequency for this rotation that scaled sublinearly with shear rate as $Wi^{0.62}$. For concentrated DNA solutions, two distinct time scales were observed: the first associated with the chain retraction dynamics (the short time scale) and the second possibly related to the dynamics of constraint release and contour length fluctuations (the long time scale). The probability distribution of chain extension broadened dramatically at high *Wi* from its approximately Gaussian shape at low *Wi*, which is not typical of pre-averaged bulk rheological theory. Robertson and Smith (2007) used optical tweezers to measure the intermolecular forces acting on a single DNA chain as exerted by the surrounding entangled molecules and found three distinct time scales: the short time scale was determined as close to the theoretical value of the Rouse time, the long time scale was associated with the disengagement time of reptation theory, and the intermediate time scale was speculated to be a second reptative process that was correlated with the dynamics of the effective reptation tube under shear.

Despite the numerous successes of single-chain microscopy to date, experimentation alone cannot resolve all of the outstanding issues that perplex rheologists at high *Wi*. The primary limitation of these experiments is the small number of molecules that can be effectively tracked simultaneously, which is especially true of dense polymer melts. A further limitation lies in the small number of flow geometries that lend themselves to direct visualization; even in steady shear flow, it is difficult to view all flow planes within the sample using the same apparatus.

Atomistic simulation of polymeric liquids offers a complementary perspective of individual chain dynamics under flow. Most nonequilibrium flow simulations to date have focused on the bulk rheological and structural properties of both atomistic [Moore *et al.* (2000); Baig *et al.* (2006); Kim *et al.* (2008a); Baig and Mavrantzas (2009); Mavrantas and Theodorous (1998); Mavrantzas and Öttinger (2002); Todd and Daivis (1998)] and coarse-grained (bead-rod and bead-spring chains) [Baig and Mavrantzas (2009); Kröger *et al.* (1993); Kröger and Hess (2000); Öttinger (1996); Doyle *et al.* (1997); Venkataramani *et al.* (2008)] liquids. Although much new insight have been garnered from these studies, possibly this focus on bulk behavior at macroscopic length and time scales has resulted in overlooking key microscopic information concerning the molecular-scale origin of the bulk rheological and structural properties. Indeed, it has sometimes led to inadequate explanations of observed bulk-scale phenomena [Kim *et al.* (2009)] as described below.

The primary advantage of simulation over experiment is that every chain within the sample can be examined individually, not only those which were optically labeled and under view in the experimental apparatus. This allows much more detailed information to be gleaned from the simulation with respect to the experiment, as statistically meaningful correlations can be established via averaging of the dynamical behavior of each individual chain. Also, simulations are readily amenable to topological analysis, extending equilibrium properties such as tube diameter, primitive path length, and number of entanglements to nonequilibrium flow situations [Kim *et al.* (2008b)]. Certainly, bulk-averaged properties, such as the conformation tensor, can still be calculated, but also with the ability to examine the effects of short time scale individual chain dynamics upon

them. Ultimately, more and better information at the microscopic scale should lead to better rheological and structural models of polymeric liquids under flow.

This article extends the analysis of a prior simulation study [Kim *et al.* (2009)] aimed at elucidating the dynamics of individual molecules comprising a linear short-chain polyethylene liquid, $C_{78}H_{158}$, under steady shearing flow. Both nonequilibrium molecular dynamics (NEMD) and Brownian dynamics (BD) simulations were performed, but on different levels of description. The NEMD simulations were conducted using the united-atom model of Siepmann *et al.* (1993) at the fine-grained atomistic level and the BD simulations were performed using a dilute solution of bead-rod chains. The atomistic-level simulations allow a direct investigation to be made of the individual chain dynamics of the linear polyethylene chains and hence into the microscopic origins of macroscopic rheological properties. Comparison between NEMD and BD simulations allows assessment of the differences between the dynamics of individual molecules that constitute dense liquids with respect to the corresponding dynamics of the similar chains in dilute solution.

II. SIMULATION METHODOLOGY

A. NEMD simulation

NEMD simulations of linear $C_{78}H_{158}$ were performed in the *NVT* ensemble using the SLLOD equations of motion of a homogeneous shear flow [Evans and Morriss (1990)], which are equivalent to the p-SLLOD equations of motion in this planar Couette flow [Edwards and Dressler (2001); Baig *et al.* (2005b); Edwards *et al.* (2006)]. The Nosé–Hoover thermostat [Nosé (1984); Hoover (1985)] was used to maintain the temperature of the liquid at a constant value of 450 K. The SLLOD equations of motion are

$$\dot{\mathbf{q}}_{ia} = \frac{\mathbf{p}_{ia}}{m_{ia}} + \mathbf{q}_{ia} \cdot \nabla \mathbf{u},$$

$$\dot{\mathbf{p}}_{ia} = \mathbf{F}_{ia} - \mathbf{p}_{ia} \cdot \nabla \mathbf{u} - \dot{\varsigma} \mathbf{p}_{ia},$$

$$\dot{\varsigma} = \frac{p_\varsigma}{Q}, \quad \dot{p}_\varsigma = \sum_i \sum_a \frac{\mathbf{p}_{ia}^2}{m_{ia}} - DNk_BT, \quad Q = DNk_BT\tau^2. \tag{1}$$

In these equations, specific molecules and atoms are distinguished with subscripts i and a, respectively. For example, $\mathbf{p}_{ia}$ denotes the momentum vector of atom a in molecule i. The symbols $\mathbf{q}_{ia}$, m_{ia}, and $\mathbf{F}_{ia}$ represent the position vector, mass, and force vector in the same fashion. The $\nabla \mathbf{u}$ is the velocity gradient tensor in the equations of motion; in the present situation, the only nonzero component is the shear rate, $\dot{\gamma}$. The variables Q, ς, and P_ς indicate the inertial mass, coordinate-like, and momentum-like variables, respectively, of the Nosé–Hoover thermostat. The k_B refers to the Boltzmann constant, and N, V, and T are the total number of atoms, the volume of the system, and the absolute temperature, respectively. The symbol D denotes the dimensionality of the system. Under planar Couette shear flow, the Lees–Edwards boundary condition [Lees and Edwards (1972)] is applied in the gradient direction, with periodic conditions with respect to the flow and vorticity directions.

The Siepmann–Karaboni–Smit [Siepmann *et al.* (1993)] united-atom model for linear alkanes was adopted in the NEMD simulations because of its extensive use for simulating equilibrium thermodynamic properties and rheological behavior of alkanes and polyethylenes. However, a bond-stretching interaction was substituted for the rigid bond in the

original united-atom model between adjacent atoms in the form of a harmonic potential function, primarily to relieve issues associated with stiff integrations at small time scales. The five types of interaction potentials present in this model are bond stretching, bond bending, bond torsion, and intramolecular and intermolecular Lennard–Jones (LJ). More details of the exact form of the model and its parameterization adopted in this study may be found in the literature [Baig *et al.* (2005a, 2006)].

In order to ensure the absence of a system-size effect, the simulation box dimensions were chosen carefully as $130.50 \times 54.00 \times 54.00$ Å^3 in xyz space, considering the fully stretched length of linear $C_{78}H_{158}$ (=99.45 Å) [Baig *et al.* (2006)]. Note that the simulation box is only extended in the direction of flow since, under shear, the chains are only approximately fully stretched at very high shear rates where they are also aligned very close to the direction of flow. The density of linear $C_{78}H_{158}$ was set to $\rho = 0.7640$ g/cm^3, as determined from experiment. Therefore, 160 molecules and 12 480 interaction sites were inserted in the simulation box. The magnitude of the averaged end-to-end vector of the test liquid at equilibrium was calculated as approximately 38 Å. The Rouse relaxation time (or the longest rotational relaxation time), τ_R, was determined at equilibrium using the KWW method [Williams and Watts (1970); Williams *et al.* (1971); Tsolou *et al.* (2005); Deschenes and van den Bout (2001)] to be roughly 2300 ps. Based on prior experience [Kim *et al.* (2008b)], the type of thermostat (atomistic or molecular [Travis *et al.* (1995); Padilla and Toxvaerd (1996)]) does not influence the simulation results at the relatively low shear rates used in this study.

B. BD simulation

BD simulations of the free-draining, bead-rod chain liquid were carried out under shear flow to assess the differences between individual molecular dynamics in dense liquids as opposed to dilute solutions. Simulations were conducted using methods described previously [Doyle *et al.* (1997); Somasi *et al.* (2002)]. The linear macromolecules were modeled as freely jointed chains possessing the same contour length as the polyethylene molecules used in the NEMD dense liquid simulations. A test chain was comprised of 24 beads connected by rods of length 4.4 Å, resulting in a maximum chain length of about 100 Å.

In the BD simulations, there were three external forces acting on the beads, which satisfy the equation

$$\mathbf{F}_i^H + \mathbf{F}_i^C + \mathbf{F}_i^B = 0, \quad i = 1,2, \ldots, N_k. \tag{2}$$

The $\mathbf{F}_i^H$, $\mathbf{F}_i^C$, and $\mathbf{F}_i^B$ represent the hydrodynamic drag force, the constraint force, and the Brownian force at the ith bead, respectively. The hydrodynamic drag force is described by Stokes drag acting on the beads

$$\mathbf{F}_i^H = -\zeta(\dot{\mathbf{r}}_i - \mathbf{v}_i^\infty), \tag{3}$$

where the ζ denotes the isotropic drag coefficient, which is related to the largest relaxation time of the model fluid. The $\dot{\mathbf{r}}_i$ and $\mathbf{v}_i^\infty$ are the velocity of the bead and streaming velocity profile at bead i, respectively. The constraint force that maintains constant bond length (a) between adjacent beads is

$$\mathbf{F}_i^C = T_i\mathbf{u}_i - T_{i-1}\mathbf{u}_{i-1},$$

$$\mathbf{u}_i = (\mathbf{r}_{i+1} - \mathbf{r}_i)/a. \tag{4}$$

T_i represents tension between the beads and $\mathbf{u}_i$ refers to the orientation of rod i. The Brownian force that describes collisions between neighboring beads is

$$\langle \mathbf{F}_i^B(t) \rangle = 0,$$

$$\langle \mathbf{F}_i^B(t)\mathbf{F}_j^B(t+\Delta t) \rangle = 2k_B T\zeta\delta_{ij}\delta(\Delta t) \approx \frac{2k_B T\zeta\delta_{ij}}{\Delta t}. \tag{5}$$

The δ represents the Dirac delta function and the δ_{ij} refers to the unit tensor.

The set of evolution equations for the position vectors of beads is obtained by combining Eqs. (3)–(5) with Eq. (2) and integration subject to the constraints

$$d\mathbf{r}_i = \left[\mathbf{v}_i^\infty + \frac{\mathbf{F}_i^C}{\zeta}\right]dt + \sqrt{\frac{2k_B T}{\zeta}}d\mathbf{W}_i, \quad i = 1,2,\ldots,N_k,$$

$$(\mathbf{r}_{i+1} - \mathbf{r}_i)(\mathbf{r}_{i+1} - \mathbf{r}_i) - a^2 = \phi^2, \quad i = 1,2,\ldots,N_k - 1, \tag{6}$$

using the iterative technique developed by Liu (1989) and proven to be optimal for this size of chains by Somasi *et al.* (2002). The $d\mathbf{W}_i$ is a Wiener process and the ϕ^2 is the specific tolerance.

The model described in the preceding paragraphs constitutes a dilute polymer solution. The BD simulations were performed by matching the longest relaxation time of the bead-rod model to the equilibrium value of the Rouse time as extracted from atomistic simulation, 2300 ps. Although the NEMD simulations were conducted with a dense liquid, the $C_{78}H_{158}$ fluid contains very few entanglements [Kim *et al.* (2008b); Foteinopoulou *et al.* (2006)]. Consequently, comparison of the NEMD and BD simulation results could lead to some interesting conclusions, since the dilute solution analysis of the BD simulations examines the individual chain dynamics of a molecule in isolation, based on the prescribed value of the Rouse time, whereas the atomistic NEMD simulations analyze the individual chain dynamics of molecules comprising a dense liquid at the same value of the Rouse time. Thus the relevant dynamical properties can be compared at equivalent values of *Wi*. This contrast between individual molecules (free-draining BD) and molecular liquids (atomistic NEMD) should reveal similarities and differences between the two cases and could lead to new insight into the universality and diversity of the dynamics of individual chains in macromolecular solutions and melts.

C. Brightness distribution for configurations of chain molecules

The dynamics of individual DNA molecules have been observed under shear using video fluorescence microscopy during the past decade [Smith and Chu (1998); Smith *et al.* (1999); LeDuc *et al.* (1999); Teixeira *et al.* (2005); Schroeder *et al.* (2005); Robertson and Smith (2007)]. In this technique, the internal configuration of the chain is related to the brightness of the signal as measured under a microscope since the individual DNA molecules are fluorescently marked. In other words, the brightness changes according to the configurational distribution of chains at a specific spatial location. For example, the coiled configuration appears brighter than other conformations because the radius of gyration of the chain is smaller.

In a similar vein to the experimental brightness measurements, the same idea has been applied to simulation data to classify numerous configurations of chain molecules and to track the configurational changes of specific molecules as a function of *Wi* [Venkatara-

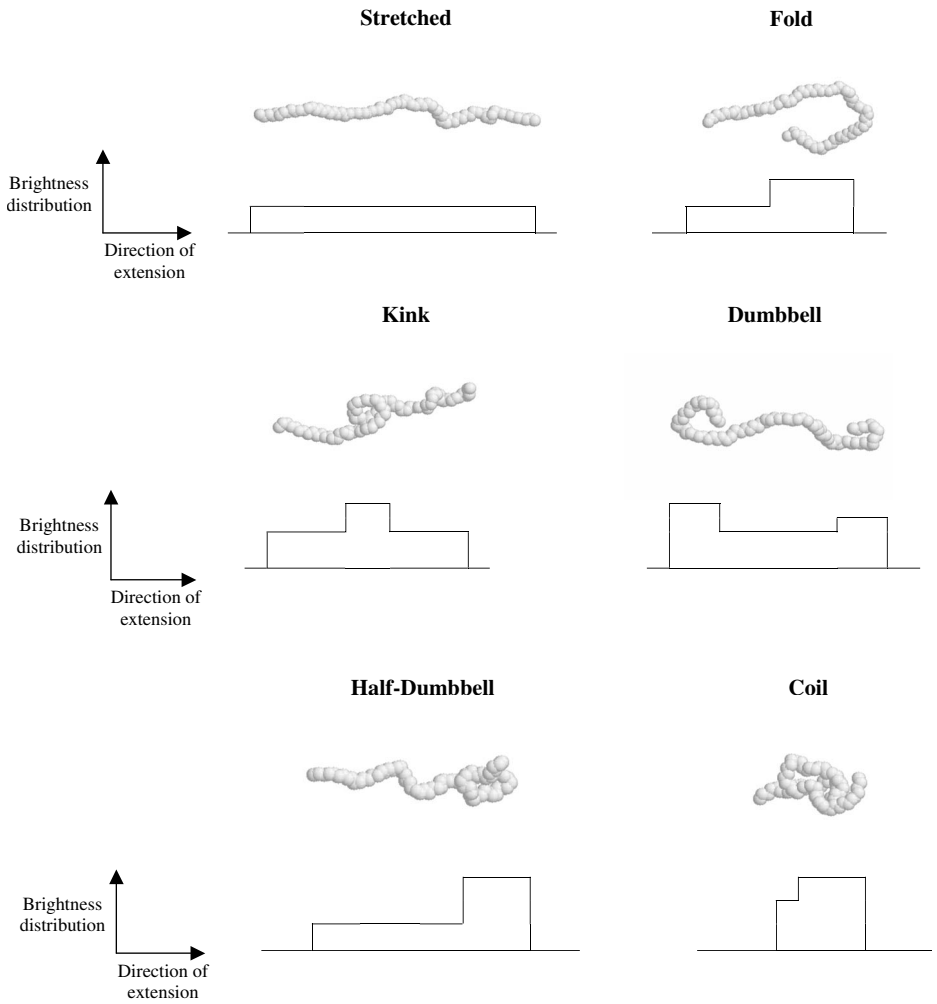

FIG. 1. Representative configuration classes of chain molecules as defined by the brightness distribution of Venkataramani *et al.* (2008).

mani *et al.* (2008)]. The analysis presented below follows exactly the scheme of Venkataramani *et al.* (2008) and will not be explained here. Figure 1 displays the configuration classes of the chain molecules considered in this work: they are, in order of increasing magnitude of the end-to-end vector, coil, fold, dumbbell, kink, half-dumbbell, and stretched.

III. RESULTS AND DISCUSSION

A. Dynamics of the end-to-end vector

NEMD simulations were performed for the liquid $C_{78}H_{158}$ at equilibrium and under shear at Wi ranging from 0.001 to 1000. A plot of the mean-squared, end-to-end vector, $\langle R^2_{ete}\rangle$, versus Wi is displayed in Fig. 2 [Kim *et al.* (2008b)]. (Note that the error bars in all cases of the atomistic simulation data presented in the figures below are approximately equal to the sizes of the symbols themselves.) This quantity provides a determination of the absolute extension of the molecules. At low values of Wi, $\langle R^2_{ete}\rangle$ assumes its quiescent

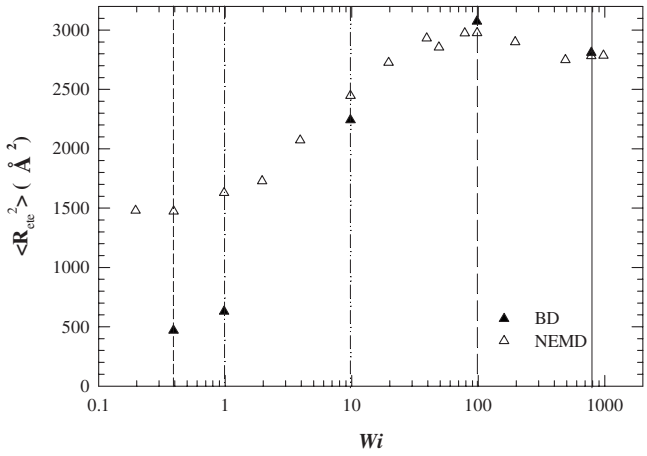

FIG. 2. The mean-square chain end-to-end distance, $\langle R^2_{\text{ete}} \rangle$, for $C_{78}H_{158}$ as a function of *Wi* from the atomistic NEMD (open symbols) and BD (filled symbols) simulations.

value of 1500 Å^2. As *Wi* approaches unity, $\langle R^2_{\text{ete}} \rangle$ begins to increase as the chain molecules begin to extend due to the hydrodynamic forces imposed by the shear field. In this *Wi* regime, the free energy change of the fluid, relative to its equilibrium value, is dominated by the entropic configurational reduction as the molecules extend, thereby drastically diminishing the number of allowable distributions of the chains' constituent atomic units. Once *Wi* increases beyond unity, the nonlinear viscoelastic regime begins, wherein the time scale of the shear flow becomes smaller than the Rouse time. As *Wi* increases from a value of 1 to about 40, a very dramatic increase is observed in $\langle R^2_{\text{ete}} \rangle$, which has traditionally been used to explain the onset of shear-thinning behavior in polymeric liquids beyond a *Wi* of unity; i.e., the deformation and preferential orientation of the chains relative to the flow direction relieves some of the hydrodynamic stress imparted to the molecular segments by the shear field. This results in a value of the shear stress that increases slower than the kinematics of the shear field would suggest.

The $\langle R^2_{\text{ete}} \rangle$ curve in Fig. 2 begins to attain a maximum at a *Wi* value of approximately 50. This behavior is unexpected based upon that of bulk-averaged rheological theories, which mandate that the chain extension should either increase continuously as *Wi* is raised or else reach a plateau value as the chains approach their maximum extension. The $\langle R^2_{\text{ete}} \rangle$ decreases substantially after attaining its maximum value of 3000 Å^2 (corresponding to a value of $|\mathbf{R}_{\text{ete}}|$ of 55 Å) at higher *Wi*, ultimately saturating at *Wi* on the order of 1000.

The NEMD simulation results for the polyethylene liquid $C_{78}H_{158}$ can be compared and contrasted to the behavior of the free-draining bead-rod chain at corresponding *Wi* using BD. In these simulations, five values of *Wi* were examined: one in the low *Wi* linear viscoelastic regime ($Wi=0.4$), at the transition to the nonlinear viscoelastic regime ($Wi=1$), during the *Wi* regime where $|\mathbf{R}_{\text{ete}}|$ is increasing dramatically ($Wi=10$), at the maximum value of $|\mathbf{R}_{\text{ete}}|$ ($Wi=100$), and at a very high value ($Wi=780$) after the maximum has been achieved.

Results of the BD simulations are also presented in Fig. 2. At the lowest two values of *Wi*, the mean-squared, end-to-end distance is much smaller than the values computed from the NEMD simulations. This is as expected since the freely jointed bead-rod model does not contain the excluded volume effect associated with the intramolecular potential

energy or any of the other four potential energy contributions either (see previous section). Hence the bead-rod chains are much more tightly coiled on average than those of the NEMD simulations, which are relatively stiff in comparison. A Kuhn step analysis of the polyethylene chains in the dense liquid reveals that seven rods would be sufficient to describe a coarse-grained version of the polyethylene molecule; however, these rods would have a length of 15 Å, which is too large to catch the fine-scale dynamics of bending that are required to assume the hairpin-like tumbling structures, as described below. (The present chains are too short for this analysis to apply in a strict sense.) Here, 23 rods of length 4.4 Å are used in order to capture the high shear rate behavior adequately and the low shear rate behavior is not of direct interest.

For all values of *Wi* beyond unity, however, $\langle R^2_{ete} \rangle$ is almost quantitatively the same between the two model liquids. Indeed, the maximum chain extension of the bead-rod chain is the same as that of the atomistic model and it occurs at the same value of *Wi*. It is very curious that these two vastly different models, one for a dense liquid and one for an infinitely dilute solution, provide the same values of $\langle R^2_{ete} \rangle$ for large values of *Wi*. Other research groups have found similar interesting behavior of molecular extension in solutions by comparing data over large variations of concentrations ranging from very dilute to semi-dilute. Hur *et al.* (2001) studied the dynamics of DNA solutions of concentrations ranging from $10^{-5}c^*$ to $6c^*$ using fluorescence microscopy. Their results for the mean fractional extension of the chain molecules indicate that this quantity is independent of concentration when it is normalized by the contour length of the molecule. The value of this extension asymptotes to a value of 0.4 at high *Wi*, which is again independent of the solution concentration. This is in contrast to the value of about 0.55 (it is the square of the extensions that appear in Fig. 2) at the maximum chain extension in the NEMD simulations of $C_{78}H_{158}$. There is no evidence of this maximum in the BD simulations of Hur *et al.* (2001). However, the critical value of *Wi* where the two simulation results show evidence of attaining a plateau (BD) or maximum (NEMD) is roughly the same value of approximately 75. Stoltz *et al.* (2006) also noticed that the fractional chain extension was independent of concentration in BD simulations of a bead-spring model representing DNA solutions at concentrations varying from infinitely dilute to $2c^*$.

The seemingly bizarre behavior of $\langle R^2_{ete} \rangle$ with *Wi* was first observed by Morriss *et al.* (1991) and later by Cui *et al.* (1996) in NEMD simulations of shear flow for liquids of n-alkanes with chain lengths up to 24 carbon atoms. Moore *et al.* (2000) performed NEMD simulations of $C_{100}H_{202}$ under shear and observed a limiting plateau value of $\langle R^2_{ete} \rangle$ at high values of *Wi*. Moore *et al.* explained the maximum by comparing the hydrodynamic pressure of the simulation to the potential LJ energy of intermolecular interactions; i.e., the energetic interactions of united-atoms on separate macromolecules. They hypothesized that it occurred due to a balance between two opposing phenomena generated by the shear field. The expected (from bulk-averaged rheological theories) deformation and orientation of the macromolecules were generated by the hydrodynamic forces at low *Wi*; however, for high values of the shear rate, they argued that the high amount of kinetic energy imparted to the atomic units of the chain molecules induces a randomizing Brownian-like collisional force, which causes the chains to retract from their overly extended configurations. Moore *et al.* based this hypothesis on the simulated behavior of the intermolecular LJ potential energy used in the SKS model. To illustrate this, Fig. 3 reproduces data of Kim *et al.* (2008b) for the intermolecular LJ potential of $C_{78}H_{158}$; the same qualitative behavior is observed for all short-chain polyethylenes simulated to date. Data display a clear decrease at low *Wi*, followed by a minimum value that corresponds to the value of *Wi* where the maximum occurs in Fig. 2. Subsequently, there

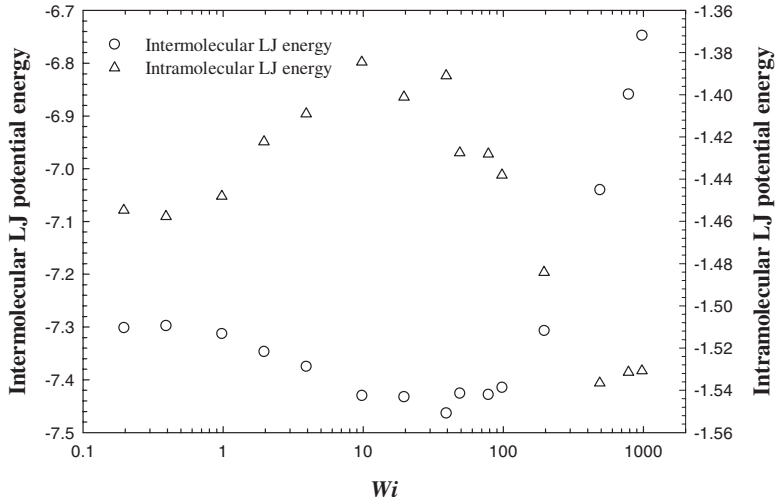

FIG. 3. The intermolecular and intramolecular LJ potential energies as functions of *Wi*.

is a very sharp rise in the LJ potential energy with increasing *Wi*. The sign convention of the energetic expressions used herein is standard: the interparticle force is negative for attraction and positive for repulsion. Therefore, the decrease in the potential energy at low *Wi* implies a situation in which the extension and preferential orientation of the chain molecules are attractive; i.e., once extended and aligned, the chains are able to pack more closely with each other. At high *Wi*, however, the potential energy becomes much more repulsive and thus the atomistic units on different chains must be revisiting their less-extended and less-oriented configurations from low values of *Wi*. The hypothesis that these repulsive forces are due to increasingly violent interactions as the kinetic energy of the atomic units is augmented by the increase in the magnitude of the imposed hydrodynamic shear force is thus a natural deduction from the intermolecular LJ energy data.

Although the data presented thus far seem to support the hypothesis of Moore *et al.* (2000), there are two inconsistencies which call into question this analysis. First, note from Fig. 3 that the values of the intermolecular LJ potential energy in the high *Wi* regime are actually smaller in absolute magnitude than the equilibrium value. This implies a more repulsive system configuration than exists under quiescent conditions and hence implies that the chain-like molecules inhabit configurations that are more entropically favorable than those which exist when there are no hydrodynamic forces within the system. This appears to contradict the principle of maximum entropy within the perspective of Moore *et al.* since a purely randomizing Brownian-like force could not produce an entropic state higher than that which is present at equilibrium. The second inconsistency can be deduced from the data of Baig *et al.* (2006), who performed NEMD simulations of planar elongational flow of the same short-chain polyethylene as modeled herein. Plots of the intermolecular LJ potential energy versus elongation rate from the cited article display a much more dramatic decrease in this energy for low and intermediate values of elongation rate as the molecules become highly extended and oriented in the direction of flow [Baig *et al.* (2006)]. At the highest values of elongation rate examined, the LJ energy reaches a plateau value that is much lower than its quiescent value. This plateau occurs as the chains attain their maximum extensions of 99 Å [Baig *et al.* (2006)]. However, at

these high values of elongation rate, the hypothesis of Moore *et al.* still mandates that Brownian-like collisional forces would cause a reduction in the extension and orientation of the chains, which is not observed in the simulation data.

Kim *et al.* (2009) recently proposed an alternative mechanism to explain the maximum observed in the $\langle R^2_{ete} \rangle$ versus Wi curve of Fig. 2. They hypothesized that the primary contributor to the observed behavior was the development of a significant degree of single-chain rotation or tumbling at high Wi. Although the system is dominated by the entropic effects at low Wi, the vorticity imposed by the shear field ultimately results in molecular chain tumbling events which occur with greater frequency, on average, with increasing Wi. As the chain tumbles, it assumes a configuration that takes on a hairpin-like structure at high Wi, which Smith *et al.* (1999) likened to pulling a rope over a pulley. This chain configuration increasingly narrows in width as Wi increases until the two chain segments (i.e., the two sides of the rope rotating around the pulley) are essentially nearest neighbors. This idea allows a rationalization of the behavior of the intermolecular LJ potential energy in shear and planar elongational flow, which was described above. Again, the entropic configurational effect dominates the system at low Wi, which induces more energetically favorable side-to-side interactions between neighboring chains. This is manifested by the decrease in the intermolecular LJ energy for low values of Wi. However, once the molecules begin to tumble with increasingly hairpin-like configurations at higher Wi, the intermolecular LJ energy increases dramatically as separate chains are effectively pushed farther away and screened from each other as different segments of the same chain pass by each other during the tumbling event. Note that these hairpin-like configurations are not present at equilibrium, which explains the fact that the intermolecular LJ energy at high Wi does not assume the equilibrium value.

Further evidence confirming this explanation is provided by examining the behavior of the intramolecular LJ potential energy, which is also displayed in Fig. 3. This energy is associated with the interactions of atoms on the same chain that are separated by more than three bonds. At low values of Wi, the intramolecular LJ energy is only marginally higher than its equilibrium value; however, it increases dramatically in the nonlinear viscoelastic regime, when $Wi > 1$, and attains a maximum at nearly the same Wi as apparent from Fig. 2. This is the expected behavior one should observe as the chain molecules extend under shear; i.e., the atoms on the same chain are pushed farther apart and hence a less negative value of the intramolecular LJ energy. At high Wi, the energy decreases dramatically, ultimately falling below its equilibrium value. This is consistent with the notion of chain tumbling, since separate segments of the chain move past each other in close proximity. Also, the exclusion of different chains from the immediate vicinity of a tumbling molecule creates a situation in which the intramolecular LJ energy must be lower than the equilibrium condition, since the atomic units of the same chain are closer together at high Wi during a tumbling event than they are under quiescent conditions. Data for the intramolecular LJ energy under planar elongational flow of Baig *et al.* (2006) displayed a monotonically increasing intramolecular LJ potential energy, which was due to the continuous stretching of the chain molecules in the flow direction.

Dunstan *et al.* (2004) performed steady shearing experiments on semi-dilute solutions of polydiacetylene 4-butoxycarbonylmethylurethane in chloroform. Optically polarized rheometry was performed on the solutions, revealing significant segmental orientation and distortion in the shear-vorticity plane. At low shear rates, the behavior of the molecules was similar to that described above, which is consistent with pre-averaged rheological theories; i.e., the chains extend and orient relative to the direction of flow. However, at higher shear rates, a maximum occurs in the segmental extension, with a subsequent decrease in this quantity with further increase of shear rate. Dunstan *et al.*

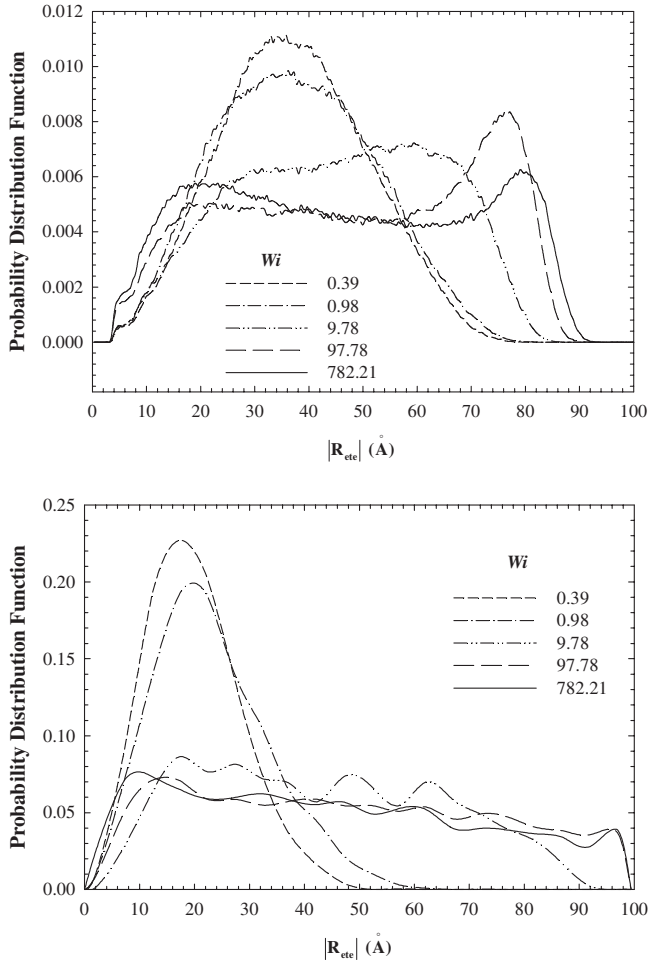

FIG. 4. Probability distributions of $|\mathbf{R}_{ete}|$ for the five values of *Wi* designated by the vertical lines in Fig. 2 as calculated in the (a) NEMD and (b) BD simulations.

described these high shear chain configurational changes as "balling," since the chains appear to become less oriented and extended as the shear rate increases beyond the maximum. However, it is evident that this bulk-average rheo-optical measurement might simply be responding to the onset of rotational motion, which reduces the ensemble average of the extension of the end-to-end vectors of the chain molecules. Note that these molecules contain a significant degree of side-chains, which could result in more coiled than hairpin-like rotation at high shear rates beyond the maximum.

Further evidence of chain tumbling is provided by Fig. 4, which displays the probability distribution of finding a chain with an end-to-end vector of a certain magnitude. The distributions at the five values of *Wi* presented in this figure correspond to the vertical lines in Fig. 2. These values of *Wi* were chosen to depict the behavior in the five regimes of interest: one in the linear viscoelastic regime, one at the transition from linear to nonlinear viscoelasticity, one in the regime of dramatically increasing chain extension, one at the maximum chain extension, and one at very high *Wi* beyond the maximum.

According to Fig. 4(a) of the NEMD simulations, the distribution at the lowest value

of $Wi=0.39$ displays the expected Gaussian behavior, with the peak centered around a value of $|\mathbf{R}_{ete}|$ that is very close to the equilibrium value of 38 Å. As Wi is increased to unity, the distribution retains its Gaussian character and the peak location shifts to higher values of $|\mathbf{R}_{ete}|$. This is the expected behavior from a pre-averaged rheological theory. However, at the same time, the peak of the distribution is decreasing in height and the whole distribution is widening. This behavior has also been observed by Morriss *et al.* (1991) for liquids decane and eicosane. These trends are not expected from pre-averaged theories and indicate that the degree of alignment around the preferred direction of orientation is diminished by the increasing hydrodynamic shear forces within the liquid. When Wi (<1) is well within the nonlinear viscoelastic regime, where the average extension of the molecules is increasing rapidly (see Fig. 2), the distribution has widened considerably and has developed a rudimentary shoulder on its left side. The peak of the distribution has continued to shift to longer values of $|\mathbf{R}_{ete}|$, corresponding to the increasing extension of the molecules. For larger values of Wi, it is apparent that the distributions become inherently bimodal, with a high "stretch" peak at large values of $|\mathbf{R}_{ete}|$, and a second "rotational" peak at low $|\mathbf{R}_{ete}|$. No hint of a rotation peak appears in the decane simulations of Morriss *et al.* (1991); however, their simulations of the longer molecule eicosane begin to display similar behavior at the highest shear rates

As the degree of chain tumbling increases with Wi, the average value of $|\mathbf{R}_{ete}|$ must decrease since this quantity must become relatively small as the chain ends of the hairpin-like structure pass each other during mid-cycle. Thus, on a time-averaged basis, the distribution is smeared to the left side of the stretch peak and to such an extent that a second rotational peak develops at high Wi. Note that the stretch peak at $Wi=782$ corresponds to $|\mathbf{R}_{ete}|\sim 80$ Å, which is approaching the maximum extension of 99 Å. Further note that the rotational peak occurs at $|\mathbf{R}_{ete}|\sim 20$ Å, which is less than the equilibrium value of 38 Å; this implies that the chain ends during the tumbling cycle are closer together on average than they are under quiescent conditions since the chain ends are tumbling with the kinked, hairpin-like configurations. At the same time, the overall average of the chain extension is determined from Fig. 2 as $|\mathbf{R}_{ete}|\sim 53$ Å, which corresponds to neither the stretch nor the rotational peak in Fig. 4(a).

Some of the characteristic behaviors of the distribution of chain lengths described above have been observed before in experiment. Teixeira *et al.* (2007) observed the widening of the distribution with shear rate in concentrated DNA solutions when individual molecular tumbling events were contributing significantly to the dynamics of the liquid. However, the mean of the distribution continuously shifted to the right, indicating a significant, continuous domination of the probability distribution by its stretching component. Smith *et al.* (1999) also observed this widening of the distribution with shear rate in their dilute DNA solutions; however, one can observe a slight degree of bimodality (which might be due to statistical error) in their distribution at the highest value of $Wi=76$ (see their Fig. 4 [Smith *et al.* (1999)]). This value of Wi is approximately the same as that at which the present simulations begin to reveal a bimodality in the distribution ($Wi\sim 80$) as evident from Fig. 4(a).

Figure 4(b) displays the corresponding probability distributions as calculated from the BD simulations at the same five values of Wi as stated above. At the lowest value of Wi, the distribution is again Gaussian. As Wi increases, the distribution begins to widen as the transition zone to the nonlinear viscoelastic region is surpassed. For high values of Wi, the distributions become extremely wide, covering almost the full range of reasonable values of $|\mathbf{R}_{ete}|$. Note that the distribution continues to extend to lower values of $|\mathbf{R}_{ete}|$ with increasing Wi, as in the NEMD simulations, and that there is a significant probability of finding chains with $|\mathbf{R}_{ete}|$ values that are lower than the equilibrium value. Although

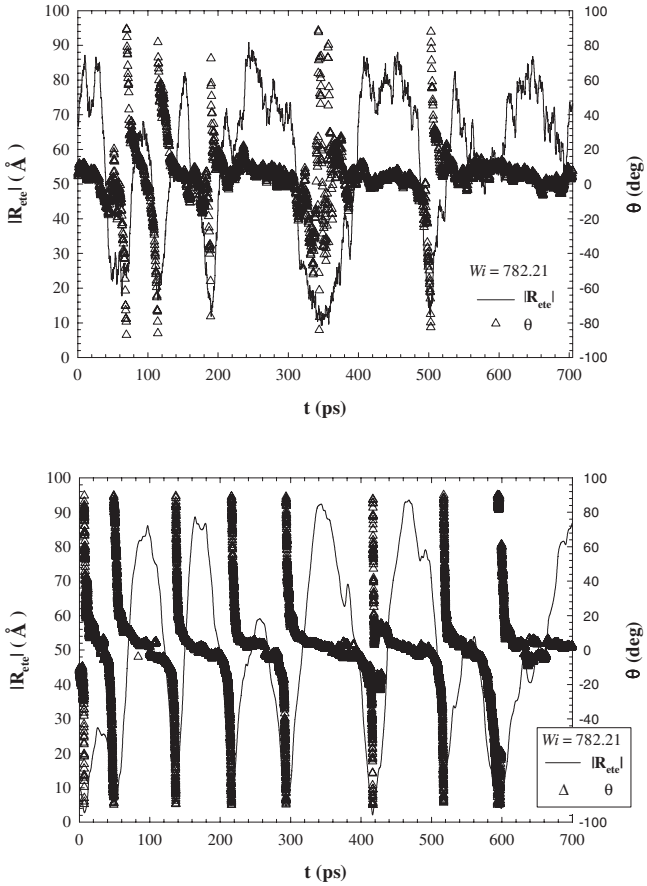

FIG. 5. The magnitude of end-to-end vector, $|\mathbf{R}_{ete}|$, and the orientation angle with respect to the flow direction, θ, as functions of time for a random chain of the (a) NEMD and (b) BD simulations.

there is no hint of bimodality in these distributions, it is readily apparent that the same physical phenomena are involved in this system: the chain molecules are tumbling between highly stretched and barely extended configurations.

The tumbling dynamics of a single, random individual chain from the NEMD simulation are displayed in Fig. 5(a) at the highest value of Wi=782. The value of $|\mathbf{R}_{ete}|$ changes dramatically with time in a quasi-periodic fashion. It oscillates between very extended chain configurations, near the fully extended length of 99 Å, and very low values that are less than the equilibrium extension of 38 Å. As demonstrated below, these low values of $|\mathbf{R}_{ete}|$ correspond to the folded configurations of the hairpin-like molecular conformations as the chain ends pass each other during a tumbling cycle. Note that $|\mathbf{R}_{ete}|$ spends more time in the stretched configurations, on average, than it does in folded conformations. Meanwhile, the orientation angle, θ, measured with respect to the direction of flow, undergoes dramatic fluctuations that correspond to the changes in the magnitude of the end-to-end vector. Indeed, the orientation angle flips sign at exactly the same times as the minima in the $|\mathbf{R}_{ete}|$ time variation. This again indicates that the chain ends approach each other very closely during the tumbling cycle. Nevertheless, the orientation angle remains at a small, positive value of approximately 5 degrees, on average, which corresponds very well to the value expected from pre-averaged rheological theo-

ries. The fact that the value of $|\mathbf{R}_{ete}|$ is essentially large on average and that the value of θ attains a value of approximately 5 degrees at high Wi explains why the pre-averaged theories give the predictions that they do. It also demonstrates that the pre-averaged theories fail to describe the small time scale tumbling dynamics of the molecules; i.e., they are coarse-grained out of the system description during the averaging process. [Baig and Mavrantzas (2009) also recently witnessed this in their multiscale simulations.] Note that this molecule spends most of its time with a positive orientation, but once it is tipped into a negative orientation, it quickly tumbles back into a positive orientation with the two ends of the chain swapping places. These negative configurational excursions are induced by either hydrodynamic or Brownian forces.

It is possible to speculate concerning the highly elliptical, hairpin-like rotation at high Wi. When viewed from a perspective involving more than one molecule, i.e., when viewing an individual molecule along with its set of nearest neighbors, it is apparent that a reptative type of dynamical mechanism is in operation, even though the liquid is not even remotely entangled. The rotating molecule is essentially diffusing through tube-like structures that are composed of the highly stretched surrounding molecules. A hydrodynamically induced Brownian excursion of a stretched chain end into a negative orientation often results in the chain diffusing out of its original tube-like structure into a similar tube below it in the flow-gradient plane. The rotating chain is essentially diffusing from a tube-like structure at a higher velocity into one directly below it with a lower velocity, just as one would expect from a rotating rigid particle suspended in a solvent undergoing shear flow. However, in the present case, the surrounding molecules inhibit the allowable chain configurations during the rotational period to those which are highly elliptical (hairpin-like).

The type of tumbling mechanism just described can, in principle, be very much different than what is observed for a liquid composed of flexible polymer chains suspended in dilute solution, as simulated using BD. $|\mathbf{R}_{ete}|$ and θ for a chain from the BD simulation at $Wi=782$ are plotted versus time in Fig. 5(b). It is evident from this figure that the tumbling of the chain molecule is again occurring in a hairpin-like configuration; however, in this case, it is apparent that the time dependence is decidedly periodic in nature rather than merely quasi-periodic as in the NEMD simulations of Fig. 5(a). This is due to the assumption of the free-draining bead-rod chain in the BD simulations, which eliminates all intermolecular effects that constrain the tumbling motion in the dense liquid of the NEMD simulations.

Plots of the components of the radius of gyrations tensor vs. time (not shown) displayed remarkable differences between rotation of the chain molecules in the NEMD and BD simulations. In the dense liquid case, the xx-component of the gyration tensor fluctuated within a relatively narrow range of values with intermediate extension. However, in the case of the free-draining chains, this component oscillated dramatically between highly extended and very low values, especially at high Wi. In both cases, the other components did not change much with time although there was a marked difference in the yy-component of the gyration tensor with the dense liquid attaining a much higher value. This suggests that the chain molecules are rotating with very different configurational motion than is suggested by Fig. 5. In the dense liquid, the chains tumble in a highly extended conformation as if on a conveyor belt. However, the free-draining chains experience an almost complete retraction or recoil collapse to a configuration that is more tightly coiled than at equilibrium during the nexus of the tumbling cycle. (This is not prohibited because of the neglect of excluded volume effects.) Further evidence of this configurational motion will be discussed below.

Figure 6 depicts the probability that a specific macromolecule has an orientation angle

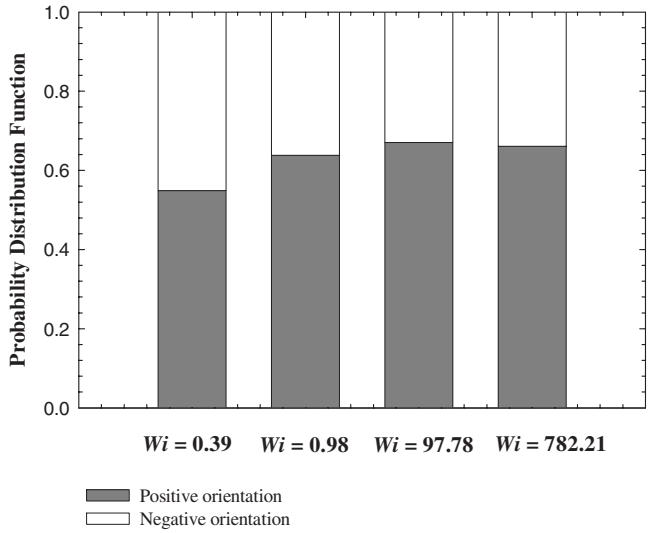

FIG. 6. Probability distribution of positive and negative end-to-end vector orientations in the dense liquids (NEMD simulations) at four values of *Wi*.

that is positive or negative. This probability is 0.5 for either positive or negative orientation under quiescent conditions. At low *Wi*, the probability of a positive orientation grows steadily in the regime where the orientation angle is dropping rapidly from the quiescent value of 45 degrees to its high *Wi* limit of about 5 degrees. This probability saturates at roughly 0.65 at high *Wi*, indicating that the theoretical pre-averaged value of the orientation angle has been attained. This confirms that the individual chain behavior displayed in Fig. 5(a) is consistent with the pre-averaged theories after the coarse-graining step (the averaging) has been performed.

BD simulations of the free-draining chains exhibited behavior that was quantitatively consistent with that of the NEMD simulations at the lowest two values of *Wi*, but the chains had a smaller probability of exhibiting a positive orientation at high *Wi* than the NEMD liquids. This is due to the fact that the BD free-draining chains are tumbling with greater frequencies at high *Wi* as expected [compare Figs. 5(a) and 5(b); also see Fig. 10 below]; therefore, on a time-averaged basis, chains spend more time inhabiting the negative quadrants. In the case of the dense liquid, Brownian forces cause the foremost chain end to dip eventually into the fourth quadrant in the gradient plane, thereby inducing a tumbling cycle. This is a less common event in the dense liquid than in the free-draining chain, since the chain end must diffuse around neighboring chains to execute the entry into the fourth quadrant.

B. Chain configurations and characteristic time scales

Figure 7 displays data for the probability density function of the possible chain configuration classes at four values of *Wi*. The configuration classes are aligned from left to right in order of increasing molecular extension of the end-to-end vector. As expected, mildly extended configurations dominate the conformational space of the macromolecules at low *Wi*. There are relatively few coil configurations relative to folded ones since these molecules are too short in length to allow the occurrence of many tightly coiled conformations, as defined by the brightness distribution described above. For these short-chain liquids, the molecules are relatively stiff, even though much longer polyethylene

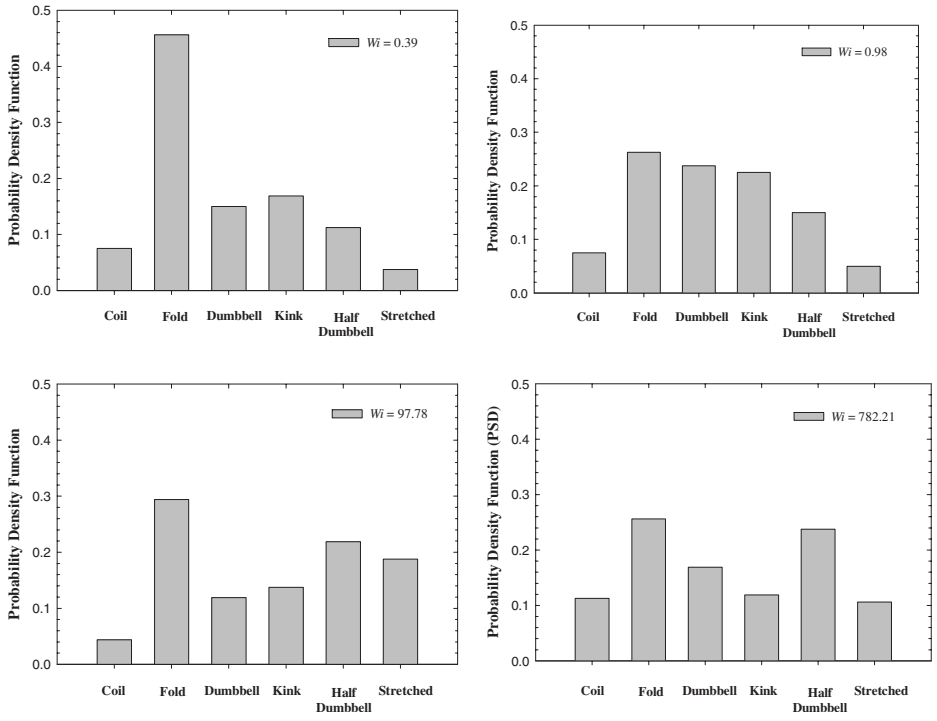

FIG. 7. Probability distribution of representative chain configuration classes in the dense liquids (NEMD simulations) at four values of *Wi*.

chains are very flexible; there are only seven Kuhn segments at equilibrium. This relative stiffness also explains the occurrence of the more highly extended configurations, half dumbbells, and stretched, even at this low value of *Wi*. However, one must keep in mind that these classifications are based on the brightness distribution defined in the previous section; in this definition, the configurations are based on shape, rather than absolute length. For example, consider two pieces of string with the same length; one is tightly stretched so that the end-to-end vector assumes its maximum value and the other has a wavy character with a small period and amplitude. Both of these strings will be classified as stretched configurations, even though the second one has a much shorter end-to-end vector than the first.

Increasing *Wi* from the linear viscoelastic regime to the transition region ($Wi \sim 1$) reduces the number of chains occupying tightly coiled or folded configurations and promotes configurations of intermediate extensions. As *Wi* increases further into the nonlinear viscoelastic regime, the number of coiled configurations is reduced further and the probability of highly extended configurations, such as half dumbbells and stretched, is dramatically increased. Even so, the probability of finding a less extended fold configuration is still significant. This is due to the fact that the chains are rotating with greater frequency and in an increasingly elliptical fashion: this demands that the fold configuration becomes more prominent. At very high *Wi*, the number of highly extended molecules continues to increase and the number of folded and coiled configurations remains approximately constant. These trends become more obvious when comparing the plots of $Wi = 0.39$ and $Wi = 782$ of Fig. 7: one again observes a rather bimodal distribution of chain configuration classes at high *Wi*, whereas it is essentially Gaussian at low *Wi*.

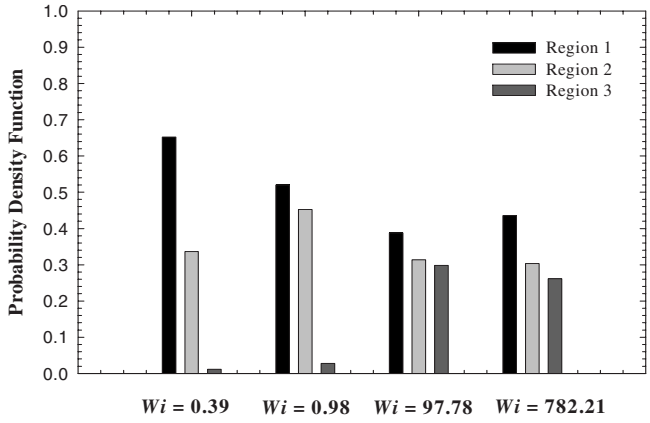

FIG. 8. Probability distribution of molecules within the three regions of $|\mathbf{R}_{ete}|$ defined in the text for the dense liquids (NEMD simulations).

Roughly the same qualitative behavior as depicted by Fig. 7 can be seen in the BD simulation data of the 15-segment bead-spring chain model of dilute macromolecular solutions of Venkataramani *et al.* (2008). Furthermore, the new BD simulations reported herein compared favorably to those of the NEMD simulations, except that there were far fewer of the relatively extended half-dumbbell and stretched configurational states near the equilibrium state; this is to be expected since the degree of extension of the chains in this *Wi* regime was much smaller than for the dense liquid due to the absence of intramolecular and intermolecular potential energies in the free-draining, bead-rod model (refer to Fig. 2). Furthermore, at high *Wi*, the free-draining solution showed a much higher percentage of coiled configurations, whereas the dense liquid chains showed a greater percentage of folded conformations. This is due to the differences in the configuration tumbling cycles (extended in the dense liquid and tightly coiled in the dilute solution) as described above.

In order to analyze further the simulation data, $|\mathbf{R}_{ete}|$ was split into three regions, relative to the distributions of Fig. 4: in units of Å, region 1, [0,40]; region 2, [40,65]; and region 3, [65–100]. These three regimes were defined relative to the distributions of the lowest (0.39) and highest (782) *Wi* that were simulated. Region 1 contains the rotational peak at high *Wi* and region 3 contains the stretch peak. At low *Wi*, regions 1 and 2 each contain about half of the stretch peak.

Figure 8 displays a histogram of the probability distribution function at the four values of *Wi* indicated on the plot for the dense liquid model used in the NEMD simulations. At the lowest value of *Wi*, the highest probability lies in region 1, with the remainder in region 2 and practically no molecules in the highly stretched region 3. There is a significant difference in the probabilities of regions 1 and 2 because the separator between these two regions is not centered at the peak (refer to preceding paragraph). At $Wi=0.98$, the probabilities in the first two regions are about equal, which is a result of the fact that the distribution function remains almost Gaussian, but the peak has shifted to a slightly higher value of $|\mathbf{R}_{ete}|$, thus making the demarcation line between regions 1 and 2 more nearly centered at the peak. Stretched chain configurations in region 3 also begin to become evident at this value of *Wi*. At $Wi=97.8$, all three regions have roughly the same probabilities, with the rotational configurational probability slightly favored; however, the stretch region 3 now has a significant probability of occurrence. As *Wi* is increased to 782, the probability of region 1 increases from its previous value at $Wi=97.8$, which is

due to the hydrodynamic augmentation of the chain tumbling dynamics; i.e., more chains are rotating and with greater frequencies, creating more folded structures on a time-averaged basis. At the same time, the number of chains in stretched configurations has decreased from the previous value of *Wi* as the molecules spend less time in stretched configurations due to the increasing frequency of the tumbling behavior.

The behavior of the chains in the BD simulations is qualitatively and quantitatively similar, except at the lowest two values of *Wi*. At those shear rates, there were almost no contributions to the regions 2 and 3 probabilities, which again reflects the lack of inter-bead repulsive forces in the free-draining chain model.

The mechanistic dynamics of the chains can be investigated through calculation of time correlation functions for the components of $\mathbf{R}_{ete}$. This allows determination of characteristic time scales intrinsic to the dynamical chain processes.

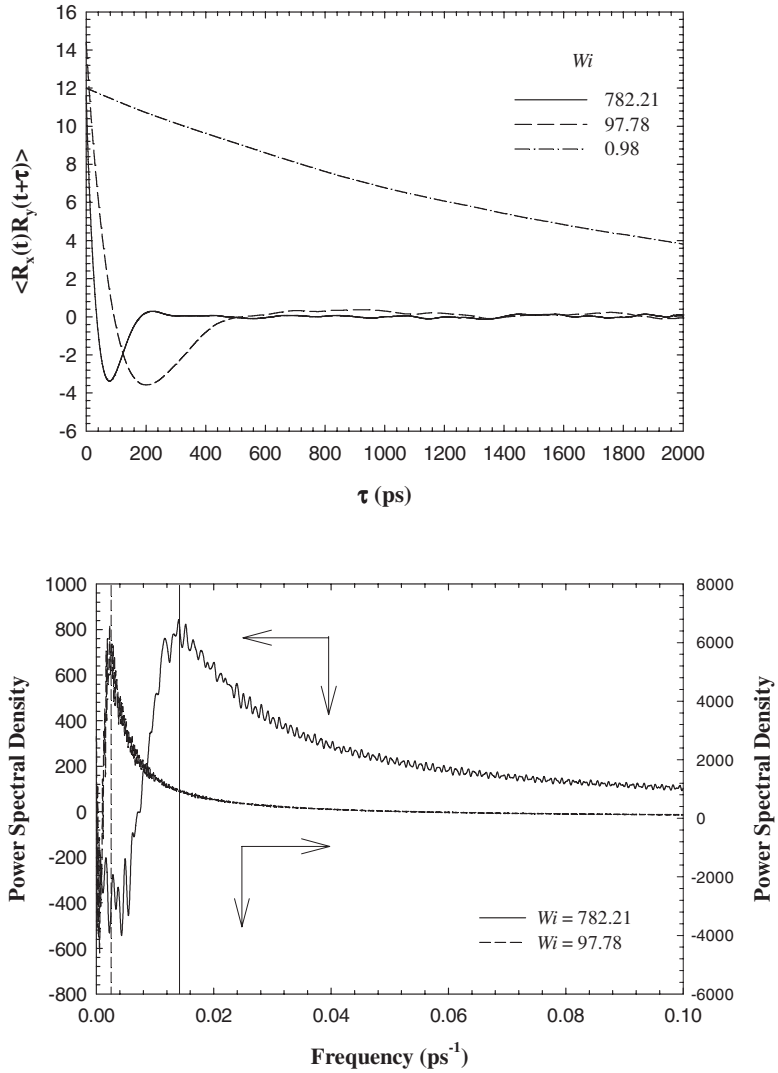

FIG. 9. Time cross-correlation functions versus observation time for three values of *Wi* and the power spectral density versus frequency for two values of *Wi* that exhibit minima in the cross-correlation function curves in the dense liquid simulations.

Aust *et al.* (2002) examined time correlations of the components of the gyration tensor for a dilute polymer solution via NEMD simulation and demonstrated that the average chain angular velocity approached the theoretical value of the vorticity $(-\dot{\gamma}/2)$ as $\dot{\gamma} \rightarrow 0$. As the shear rate increased, the chain became increasingly elongated and its angular velocity dropped relative to the vorticity of the shear field [Aust *et al.* (2002)].

Figure 9(a) displays data for the correlation $\langle R_x(t)R_y(t+\tau)\rangle$ with respect to observation time at values of $Wi=0.98$, 97.8, and 782 for the dense liquid NEMD simulations. Note that the correlations $\langle R_x(t)R_x(t+\tau)\rangle$ and $\langle R_y(t)R_y(t+\tau)\rangle$ displayed the same qualitative behavior as indicated in the figure and that similar plots were obtained at all values of Wi investigated. Cross correlations between other off-diagonal pairs of components of $\mathbf{R}_{\text{ete}}$ exhibited no correlations. These data reveal definite correlations between certain components of $\mathbf{R}_{\text{ete}}$, with characteristic time scales that are dependent on Wi. At low values of Wi, within the linear viscoelastic regime, the typical behavior is observed in which the chain relaxation is dominated by the longest relaxation time, τ_R. However, for $Wi>2$, the correlation curves each exhibit a characteristic minimum, followed by a local maximum, and then a damped oscillatory behavior at longer times; this behavior is indicative of characteristic time scales beyond the Rouse time. The free-draining chain model exhibited the same features.

These time scales can be quantified using the power spectral density, which is displayed in Fig. 9(b), through Fourier transformation of the correlation signal. With respect to the dynamics of $\mathbf{R}_{\text{ete}}$, it is evident that the correlations describe various aspects of the dynamics of the rotation motion of the chains. Characteristic frequencies can be determined from the maxima in the power spectral density curves, as indicated in the figure.

Figure 10 displays data for the intrinsic time scales associated with the dynamical chain motion: τ_R, the Rouse time (horizontal line), as well as τ_{xx}, τ_{xy}, τ_{yy}, and τ_{conv}, as functions of Wi from both the NEMD and BD simulations. The τ_{ii} are associated with the

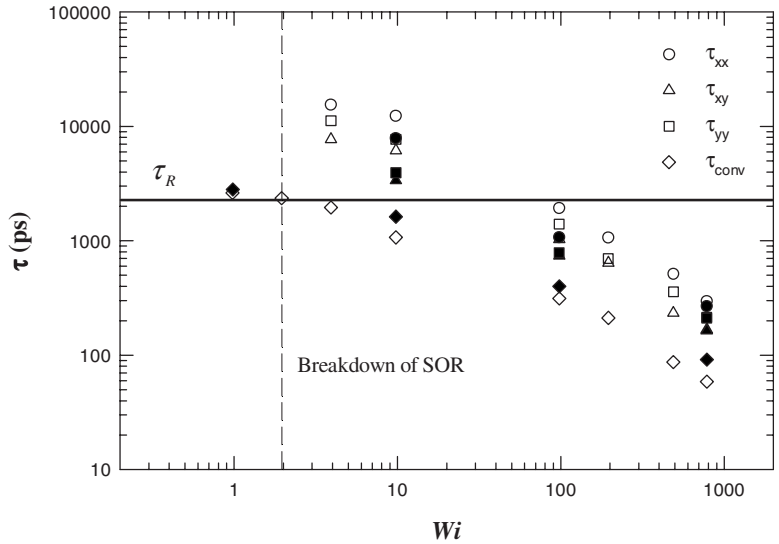

FIG. 10. Characteristic time scales versus Wi. Horizontal line represents the Rouse time. Vertical dashed line represents the value of Wi at which the stress-optical rule begins to breakdown in simulations of $C_{50}H_{102}$. Diamonds represent the time scale of relaxation of the extended molecules and all other symbols represent the time scales associated with the various auto and cross correlations of the end-to-end vector. Solid symbols represent dilute solution data and unfilled symbols denote dense liquid data.

correlations of the corresponding components of $\mathbf{R}_{ete}$, as defined above. These time scales are expected to be associated with various aspects of the chain rotation, such as the tumbling frequency, wagging motion, etc. Although these time scales are slightly different for the various components of $\mathbf{R}_{ete}$, it is not evident what are their exact interpretations; presumably, each represents a distinct facet of the chain tumbling dynamics, which is not apparent at the present time. Since $\mathbf{R}_{ete}$ has both magnitude and direction, it is possible that these small differences arise due to the stretch contribution (i.e., the magnitude) of $\mathbf{R}_{ete}$ rather than its directional contribution. Furthermore, the ensemble average of any component of $\mathbf{R}_{ete}$, which is performed when calculating the correlation $\langle R_x(t)R_y(t+\tau)\rangle$, for example, is weighted toward molecules of high extension. To investigate this issue, correlations were also computed in terms of the unit vector, $\mathbf{u} = \mathbf{R}_{ete}/|\mathbf{R}_{ete}|$, in which each molecule is weighted equally, regardless of its length. These correlations, such as $\langle u_x(t)u_y(t+\tau)\rangle$, should eliminate any stretch contribution to the intrinsic time scales that are manifested through the correlations; however, no statistically discernable difference was noted between these correlations and the data presented in Fig. 10.

The time scale τ_{conv} is assumed to correspond with the relaxation of the stretched chain configurations, which may be associated with the convection and deformation of the tube-like structures, described above, which are formed by neighboring chains that are almost fully stretched. These time scales can be quantified by assuming that the R_xR_x correlation bears the functional form of $A\exp(-t/\tau_{conv})\cos(2\pi t/\tau_{xx})$, where A is a constant. From this expression, at equilibrium, $\tau_{xx}\to\infty$, so that $\tau_{conv}\to\tau_R$. As $\tau_{conv}\to\infty$, the motions of the chains would become purely tumbling, similarly to rigid rods.

Using this assumed expression, as the shear rate decreases toward zero from a finite value, the τ_{ii} assume values between 5 and 10 times the Rouse time. For $Wi<2$, one can no longer observe minima in the time correlations of $\mathbf{R}_{ete}$, implying that the rotational time scales are no longer evident in the system response. [Note that this value of $Wi=2$ corresponds to the profile in Fig. 4(a) where the distribution became non-Gaussian.] This is caused by the low degree of vorticity in the flow field, which inhibits the excursions of the molecules into negative orientations. In other words, at low values of *Wi*, the dynamics are dominated by the deformation of the macromolecules because the shear flow has a time scale greater than the Rouse time (i.e., $1/\dot{\gamma}$), implying that the rotational motion is insignificant relative to the dynamics of the deforming chains. Apparently, the Brownian-like fluctuations induced by the shear forces are only capable of deforming the molecules in this *Wi* regime and can only induce fluctuations that lead to tumbling once the molecules are at least partially extended and, more importantly, oriented near to the flow direction. Once the chains are oriented near to the flow direction (about 5 degrees) at high *Wi*, it is easier for random Brownian-like forces to induce the chain orientation to progress into the fourth quadrant, thus initiating a tumbling cycle. At low shear rates, the orientation of the deformed chains is above 15 degrees, which makes it relatively difficult for a Brownian excursion into the negative quadrant.

In principle, the rotational time scales should approach infinity as *Wi* approaches zero. However, one cannot obtain values of these time scales for $Wi<1$ because the chain ends decorrelate on the order of the shorter Rouse time: since the chain configurations are already decorrelated, it is impossible to calculate a longer time scale. Thus, at low values of *Wi*, only the Rouse time is evident in the relaxational response of the liquid.

As *Wi* increases into the nonlinear viscoelastic regime, all of the rotational time scales are reduced dramatically until they have decreased below the Rouse time; this indicates a higher frequency of tumbling and induces the first peak in the distributions of Fig. 4(a). Thus at high shear rates, the rotational motion of the chains dominates the system re-

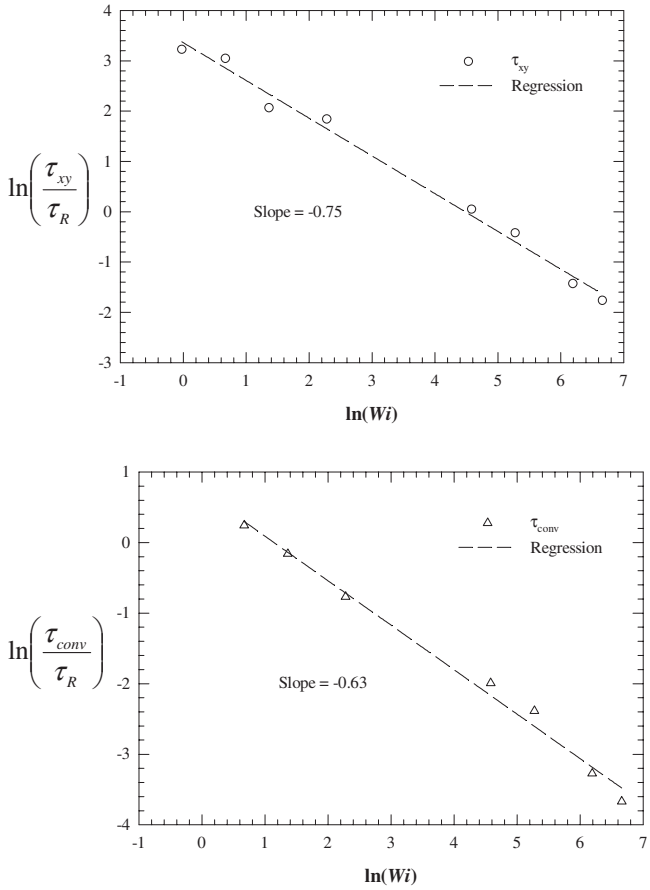

FIG. 11. Log-log plots of the characteristic time scales, relative to the Rouse time, versus *Wi* for the NEMD simulations. Note that plots of the characteristic frequencies would possess slopes of opposite sign but of the same absolute values as those presented in the figures.

sponse. The time scale τ_{conv} is equivalent to τ_R at low shear rates, but then also decreases substantially at higher shear rates. Presumably, this quantifies the affect of the flow kinematics on the convection and orientation of the reptative tube network within the fluid; i.e., as the chains become stretched to their maximum lengths, they form highly oriented, tube-like structures between neighboring stretched chains, which allow freer rotation of other chains occupying the same vicinity. All of these time scales possess power-law behavior with *Wi*, as discussed below in reference to Fig. 11.

Recent experiments of semi-dilute and concentrated DNA solutions have revealed multiple time scales associated with the kinematics of shear flow [Teixeira *et al.* (2007); Robertson and Smith (2007)]. Teixeira *et al.* (2007) observed two distinct time scales, in addition to the Rouse time, for their most concentrated solution; however, for unentangled solutions of lower concentration, they observed only a single time scale. For the highly entangled solution, they observed a ratio of the slow to fast time scales of approximately 50. Furthermore, the fast time scale was roughly a factor of 10 higher than the estimated Rouse time and was attributed to chain retraction. Robertson and Smith (2007) recorded three distinct time scales, each differing from the next by 1 order of magnitude. The shortest time scale was estimated as the Rouse time, the longest time

scale was associated with the disengagement time of reptation theory, and the intermediate time scale was related to a second reptative phenomenon that was correlated with the dynamics of the effective reptation tube. The ratio of the tube dynamics (the intermediate) time scale to the Rouse time was roughly 12 [Robertson and Smith (2007)], which is of comparable magnitude to the factor determined by Teixeira *et al.* (2007). Although the liquids simulated in the present study are not even remotely entangled, the rotational time scales are roughly a factor of 6 higher than either the Rouse time or τ_{conv} at all values of *Wi*. Given the differences in the entangled solutions and the unentangled liquids examined herein, it is difficult to compare directly experiment and simulation. However, in the present case, it does appear that the faster time scale, τ_{conv}, is associated with some sort of constraint release through the formation of tube-like structures which allow some molecules to tumble more freely with respect to almost fully stretched surrounding chains in the NEMD simulations. Recall that this time scale is associated with the decay of the correlation between configurations at a specified time with those of later times. Consequently, data of Fig. 10 indicate that this correlation dies out faster at higher *Wi* values than it does in the linear viscoelastic regime; i.e., the molecular configurations become statistically independent at a faster rate when the shear rate is high. This is reasonable since smaller segments of the chain molecules become dynamically active as *Wi* is increased, thus providing additional degrees of freedom to the chain's overall configurational state.

It is very interesting that the NEMD and BD simulations appear to yield similar characteristic time scales despite the large conceptual differences in the models used in the computations. The BD simulations show faster rotational time scales, which correspond to greater frequencies of rotation. This is to be expected since the free-draining chain model is not constrained by the presence of surrounding macromolecules. It is interesting that the convected time scale, τ_{conv}, is also apparent in the BD simulations, which could support the hypothesis that this time scale is associated with the enhanced configurational dynamics at high *Wi* of the stretched chain configurations as opposed to the configurations present during the tumbling cycle, whether in the free-draining solution or the dense liquid. Note that the difference in τ_{conv} between the NEMD and BD simulations is not assured to be statistically significant based on the present analysis; however, the trend of the data in Fig. 10 suggests that the correlation time is longer for the free-draining chains than it is for the dense liquid. To explain this observation, one can recall the argument presented above concerning the *Wi* dependence of the segmental dynamics: as the shear rate increases, smaller chain segments become dynamically active and contribute to the configuration constraint release. In the free-draining chain simulations, the course-graining procedure dictates the constant bond length between beads, thus permanently freezing the small segmental dynamics beyond a certain limit. Once this limit is achieved, increasing *Wi* further does not contribute any additional degrees of freedom to the configurational chain decorrelation, thus effectively slowing down the decay of the correlation relative to the atomistic chain model used in the NEMD simulations.

An additional explanation for the more rapid decay of the correlation in the NEMD simulation of the dense liquid can be rationalized on the basis of Fig. 5. Recall that the dense liquid displayed only quasi-periodic temporal behavior of the end-to-end vector cycles, whereas the free-draining chain solution experienced a more regular periodic tumbling cycle. Consequently, it is apparent that the dense liquid should exhibit a faster rate of decorrelation than the free-draining liquid, leading to a smaller τ_{conv} time scale.

Hence another possible interpretation of the simulation data is that the τ_{ii} characterize the rotational frequencies of the tumbling molecules and τ_{conv} quantifies the time scale over which the correlation in the rotational motion decays.

Another interesting observation from Fig. 10 is the apparent correlation between the appearance of the rotational time scales, the deviation of the Rouse time from its equilibrium value, and the onset of the breakdown in the stress-optical rule observed for a similar liquid ($C_{50}H_{102}$) by Baig *et al.* (2007). The rotational time scales and the deviation from the Rouse time appear well beyond the transition between the linear and nonlinear viscoelastic regimes ($Wi=1$). A plausible hypothesis then is that the breakdown in the stress-optical rule under shear is caused by the tumbling motion of the macromolecules, which also could be partially responsible for the shear-thinning behavior; i.e., not only are the stretched configurations of the chains relieving the hydrodynamic stresses induced by the shear, but the chain tumbling is also offering some relief.

The data of the τ_{ii} and τ_{conv} presented in Fig. 10 appear to follow power-law behavior at high Wi. Figure 11 displays this power-law dependence of the NEMD simulations using graphs of $\ln(\tau_{xy}/\tau_R)$ and $\ln(\tau_{\text{conv}}/\tau_R)$ with respect to $\ln Wi$. (The regression of the time scales τ_{xx} and τ_{yy} revealed essentially the same results as that of τ_{xy}.) The power-law exponent of τ_{xy} was calculated as -0.75 over the entire data range without much deviation from the norm. If this rotational time scales were scaling linearly with shear rate, this exponent would have been -1.0; consequently, it is apparent that the molecules within the sheared liquids are not tumbling with frequencies that are determined by the hydrodynamically imposed vorticity of the flow field. This is most likely due to the fact that over a small period of time, many of the liquid molecules are almost fully stretched at high values of Wi and are not in the process of tumbling. As mentioned above, these fully stretched molecules dominate the statistically based averages and could account for this discrepancy between the vorticity and the tumbling frequency; however, this type of sublinear scaling has been observed experimentally. Teixeira *et al.* (2005) observed a tumbling frequency in dilute DNA solutions that scaled as $Wi^{-0.62}$. Hence the chain tumbling frequency does not necessarily need to match the vorticity; however, as these solutions were dilute, it is still likely that the background solvent was evolving as dictated by the local kinematics. In other words, although the isolated chains were tumbling at frequencies other than the vorticity, the local solvent was experiencing the vorticity demanded by the shear field, barring hydrodynamic interactions between the macromolecule and the solvent. A similar regression of the BD simulation of the free-draining chain modeled in this study yielded a characteristic tumbling frequency that scaled with a factor of -0.68.

In the NEMD simulations of the dense liquid, however, the situation is more complicated by the fact that there is no solvent and the molecules are not isolated. In this circumstance, the hydrodynamic field is solely due to the molecules themselves, not the surrounding solvent. It is also evident from Fig. 11 that τ_{conv} scales sublinearly as $Wi^{-0.63}$, as fitted to a truncated Spriggs power-law equation in which $\tau_{\text{conv}}=\tau_R$ when $Wi<1$ and $\tau_{\text{conv}}=\tau_R Wi^{\alpha}$ when $Wi>1$. This value is very close to the value of -0.62 observed in the experiments of Teixeira *et al.* (2005). The BD simulations of the present study provided a scaling exponent of -0.66. This fact is either a coincidence or hints at some underlying universal connection between the tumbling frequencies and the deformation and orientation of macromolecular chains under shear.

Partial rationalization of the similarity in the NEMD and BD results is provided by the realization that the relatively short, stiff chains in the dense liquid are not tightly coiled at equilibrium, whereas the chains in the free-draining model are assumed to be ideal with no interactions between the beads. According to the Flory theorem, macromolecules in

dense polymer melts behave like ideal chains, similarly to dilute solutions at the theta temperature. Although the short-chain polyethylene liquid examined here is not a fully entangled system, it is still likely that the same type of screening of the long-range interactions (between beads of the same chain separated by three or more bonds) of a particular chain by neighboring and interpenetrating chains. Were the system entangled, however, it is highly likely that this quantitatively similar scaling behavior would not be evident.

Several groups of researchers have postulated a deformational dependence of the longest relaxation time, τ_R, under application of an external flow field [Marrucci (1996); Souvaliotis and Beris (1992); Apelian *et al.* (1988)]. For example, Souvaliotis and Beris (1992) postulated the functional form of $\tau_{\text{conv}} = \tau_R(\text{tr}\,\mathbf{c}/3)^k$, where k is a negative constant and $\mathbf{c}$ is the conformation tensor, which was mentioned in Sec. I. This power-law dependence of the relaxation time was then inserted into the pre-averaged upper-convected Maxwell model and allowed for the prediction of shear thinning in the shear viscosity. However, any connection between molecular tumbling and the degree of molecular deformation and orientation is lost through this procedure and only the pre-averaged contributions on the longest time scale will be evident in the macroscopic model behavior. Clearly, pre-averaged theories have little possibility of capturing the dynamical tumbling phenomena that are occurring at very small time and length scales.

IV. SUMMARY

In this article, we carried out NEMD simulations of the dense liquid composed of linear polyethylene chains, $C_{78}H_{158}$, to examine motion of individual molecules as a function of shear rate. BD simulations were also performed on an equivalent free-draining bead-rod model to examine the differences between dense liquid and dilute solution behavior. The mean-squared, end-to-end vector, $\langle R_{\text{ete}}^2 \rangle$, was shown to increase from its equilibrium value to attain a maximum at high shear rates. Moore *et al.* (2000) hypothesized that this effect was due to a competition between chain stretch and alignment and a Brownian-like collisional force. However, the present study suggested that the rotational motion of the chain molecules is primarily responsible for this peculiar behavior.

Both NEMD and BD simulations revealed a probability distribution of $|\mathbf{R}_{\text{ete}}|$ that was Gaussian at low Weissenberg number (Wi); however, non-Gaussian behavior was evident at intermediate values of Wi, in contrast to the predictions of pre-averaged theories. At high Wi, the NEMD distribution was bimodal, with two distinct peaks associated with rotation (low Wi peak) and stretching (high Wi peak). The BD simulations of the free-draining chain exhibited a non-Gaussian and very wide distribution of chain lengths, with the absolute width increasing dramatically with increasing Wi as chain rotation became increasingly significant.

Time trajectories of individual chain $|\mathbf{R}_{\text{ete}}|$ values and orientation angles revealed a dramatic onset of tumbling behavior of the chains at a critical Wi (~ 2). Auto-correlations and cross-correlations between the components of $\mathbf{R}_{\text{ete}}$ revealed characteristic frequencies of molecular rotation, which scaled as $Wi^{-0.75}$ power. Furthermore, after a critical Wi of approximately 2, another characteristic time scale appeared which scaled as $Wi^{-0.63}$. This was associated with a dramatic decrease in the elastic time scale of the system, which was apparently associated with the relaxation of rotational constraints and the correlation of the tumbling cycles (resulting in the first peak of the bimodal probability distribution) due to the formation of loosely defined, tube-like structures of fully stretched neighboring chains (comprising the second peak of the distribution). Although the free-draining solu-

tion is very different in character than the dense liquid, the BD simulations revealed a similar behavior, with the characteristic time scales mentioned above scaling as $Wi^{-0.68}$ and $Wi^{-0.66}$, respectively.

Individual chain configurations were explored as functions of Wi and $|\mathbf{R}_{ete}|$; NEMD and BD simulations provided similar results at high values of Wi, both qualitatively and quantitatively. At low values of $|\mathbf{R}_{ete}|$, the chain configurations were predominantly coiled at low Wi and folded at high Wi, indicating increasingly hairpin-like rotation with growing shear strength. At high values of $|\mathbf{R}_{ete}|$, the chain configurations were essentially either fully stretched or of half-dumbbell nature at high Wi, thus constituting a loose network of tube-like structures.

ACKNOWLEDGMENTS

The authors gratefully acknowledge Dr. V. Venkataramani for help with the BD simulations reported in this article. This work was made possible by the National Science Foundation under Grant No. CBET-0742679 by using the resources of the PolyHub Virtual Organization.

References

Apelian, M. R., R. C. Armstrong, and R. A. Brown, "Impact of the constitutive equation and singularity on the calculation of stick-slip flow: The modified upper-convected Maxwell model (MUCM)," J. Non-Newtonian Fluid Mech. **27**, 299–321 (1988).

Aust, C., S. Hess, and M. Kröger, "Rotation and deformation of a finitely extendable flexible polymer molecule in a steady shear flow," Macromolecules **35**, 8621–8630 (2002).

Baig, C., B. J. Edwards, and D. J. Keffer, "A molecular dynamics study of the stress-optical behavior of a linear short-chain polyethylene melt under shear," Rheol. Acta **46**, 1171–1186 (2007).

Baig, C., B. J. Edwards, D. J. Keffer, and H. D. Cochran, "A proper approach for nonequilibrium molecular dynamics simulations of planar elongational flow," J. Chem. Phys. **122**, 114103 (2005a).

Baig, C., B. J. Edwards, D. J. Keffer, and H. D. Cochran, "Rheological and structural studies of liquid decane, hexadecane, and tetracosane under planar elongational flow using nonequilibrium molecular dynamics simulations," J. Chem. Phys. **122**, 184906 (2005b).

Baig, C., B. J. Edwards, D. J. Keffer, H. D. Cochran, and V. A. Harmandaris, "Rheological and structural studies of liquid polyethylenes under planar elongational flow using nonequilibrium molecular dynamics simulations," J. Chem. Phys. **124**, 084902 (2006).

Baig, C., and V. G. Mavrantzas, "Multiscale simulation of polymer melt viscoelasticity: Expanded-ensemble Monte Carlo coupled with atomistic nonequilibrium molecular dynamics," Phys. Rev. B **79**, 144302 (2009).

Bird, R. B., R. C. Armstrong, and O. Hassager, *Dynamics of Polymeric Liquids* (Wiley, New York, 1987a), Vol. I.

Bird, R. B., C. F. Curtiss, R. C. Armstrong, and O. Hassager, *Dynamics of Polymeric Liquids* (Wiley, New York, 1987b), Vol. II.

Cui, S. T., S. A. Gupta, P. T. Cummings, and H. D. Cochran, "Molecular dynamics simulations of the rheology of normal decane, hexadecane, and tetracosane," J. Chem. Phys. **105**, 1214–1220 (1996).

Deschenes, L. A., and D. A. van den Bout, "Single-molecule studies of heterogeneous dynamics in polymer melts near the glass transition," Science **292**, 255–258 (2001).

Doi, M. and S. F. Edwards, *The Theory of Polymer Dynamics* (Oxford university Press, New York, 1986).

Doyle, P. S., E. S. G. Shaqfeh, and A. P. Gast, "Dynamic simulation of freely draining flexible polymers in steady linear flows," J. Fluid Mech. **334**, 251–291 (1997).

Dunstan, D. E., E. K. Hill, and Y. Wei, "Direct measurement of polydiacetylene 4-butoxycarbonylmethylurethane segment orientation and distortion in shear: Semidilute solutions," Macromolecules **37**,

1663–1665 (2004).
Edwards, B. J., C. Baig, and D. J. Keffer, "A validation of the p-SLLOD equations of motion for homogeneous steady-state flows," J. Chem. Phys. **124**, 194104 (2006).
Edwards, B. J., and M. Dressler, "A reversible problem in non-equilibrium thermodynamics: Hamiltonian evolution equations for non-equilibrium molecular dynamics simulations," J. Non-Newtonian Fluid Mech. **96**, 163–175 (2001).
Evans, D. J., and G. P. Morriss, *Statistical Mechanics of Nonequilibrium Liquids* (Academic, London, 1990).
Foteinopoulou, K., N. C. Karayiannis, V. G. Mavrantzas, and M. Kröger, "Primitive path identification and entanglement statistics in polymer melts: Results from direct topological analysis on atomistic polyethylene models," Macromolecules **39**, 4207–4216 (2006).
Hoover, W. G., "Canonical dynamics: Equilibrium phase-space distributions," Phys. Rev. A **31**, 1695–1697 (1985).
Hur, J. S., E. S. G. Shaqfeh, H. P. Babcock, D. E. Smith, and S. Chu, "Dynamics of dilute and semidilute DNA solutions in the start-up of shear flow," J. Rheol. **45**, 421–450 (2001).
Islam, M. T., J. Sanchez-Reyes, and L. A. Archer, "Step and steady shear responses of nearly monodisperse highly entangled 1,4-polybutadiene solutions," Rheol. Acta **42**, 191–198 (2003).
Kim, J. M., B. J. Edwards, B. Khomami, and D. J. Keffer, "Single-chain dynamics of linear polyethylene liquids under shear flow," Phys. Lett. A **373**, 769–772 (2009).
Kim, J. M., D. J. Keffer, and B. J. Edwards, "Visualization of conformational changes of linear short-chain polyethylenes under shear and elongational flows," J. Mol. Graphics Modell. **26**, 1046–1056 (2008a).
Kim, J. M., D. J. Keffer, M. Kröger, and B. J. Edwards, "Rheological and entanglement characteristics of linear chain polyethylene liquids in planar Couette and planar elongational flows," J. Non-Newtonian Fluid Mech. **152**, 168–183 (2008b).
Kröger, M., and S. J. Hess, "Rheological evidence for a dynamical crossover in polymer melts via nonequilibrium molecular dynamics," Phys. Rev. Lett. **85**, 1128–1131 (2000).
Kröger, M., W. Loose, and S. J. Hess, "Rheology and structural changes of polymer melts via nonequilibrium molecular dynamics," J. Rheol. **37**, 1057–1079 (1993).
Larson, R. G., *Constitutive Equations for Polymer Melts and Solutions* (Butterworths, London, 1988).
Larson, R. G., *The Structure and Rheology of Complex Fluids* (Oxford University Press, New York, 1999).
LeDuc, P., C. Haber, G. Bao, and D. Wirtz, "Dynamics of individual flexible polymers in a shear flow," Nature (London) **399**, 564–566 (1999).
Lees, A. W., and S. F. Edwards, "Computer study of transport processes under extreme conditions," J. Phys. C **5**, 1921–1928 (1972).
Liu, T. W., "Flexible polymer chain dynamics and rheological properties in steady flows," J. Chem. Phys. **90**, 5826–5842 (1989).
Marrucci, G., "Dynamics of entanglements: A nonlinear model consistent with the cox-merz rule," J. Non-Newtonian Fluid Mech. **62**, 279–289 (1996).
Mavrantzas, V. G., and D. N. Theodorous, "Atomistic simulation of polymer melt elasticity: Calculation of the free energy of an oriented polymer melt," Macromolecules **31**, 6310–6332 (1998).
Mavrantzas, V. G., and H. C. Öttinger, "Atomistic Monte Carlo simulations of polymer melt elasticity: Their nonequilibrium thermodynamics generic formulation in a generalized canonical ensemble," Macromolecules **35**, 960–975 (2002).
Mhetar, V. R., and L. A. Archer, "A new proposal for polymer dynamics in steady shearing flows," J. Polym. Sci., Part B: Polym. Phys. **38**, 222–233 (2000).
Moore, J. D., S. T. Cui, H. D. Cochran, and P. T. Cummings, "A molecular dynamics study of a short-chain polyethylene melt. I. Steady-state shear," J. Non-Newtonian Fluid Mech. **93**, 83–99 (2000).
Morriss, G. P., P. J. Daivis, and D. J. Evans, "The rheology of n alkanes: Decane and eicosane," J. Chem. Phys. **94**, 7420–7433 (1991).
Nosé, S., "A molecular dynamics method for simulations in the canonical ensemble," Mol. Phys. **52**, 255–268 (1984).
Öttinger, H. C., *Stochastic Processes in Polymeric Fluids* (Springer, New York, 1996).
Padilla, P., and S. Toxvaerd, "Simulating shear flow," J. Chem. Phys. **104**, 5956–5963 (1996).

Robertson, R. M., and D. E. Smith, "Direct measurement of the intermolecular forces confining a single molecule in an entangled polymer solution," Phys. Rev. Lett. **99**, 126001 (2007).

Schroeder, C. M., R. E. Teixeira, E. S. G. Shaqfeh, and S. Chu, "Characteristic periodic motion of polymer in shear flow," Phys. Rev. Lett. **95**, 018301 (2005).

Siepmann, J. I., S. Karaborni, and B. Smit, "Simulating the critical behavior of complex fluids," Nature (London) **365**, 330–332 (1993).

Smith, D. E., H. P. Babcock, and S. Chu, "Single-polymer dynamics in steady shear flow," Science **283**, 1724–1727 (1999).

Smith, D. E., and S. Chu, "Response of flexible polymers to a sudden elongational flow," Science **281**, 1335–1340 (1998).

Somasi, M., B. Khomami, N. J. Woo, J. S. Hur, and E. S. G. Shaqfeh, "Brownian dynamics simulations of bead-rod and bead-spring chains: Numerical algorithms and coarse-graining issues," J. Non-Newtonian Fluid Mech. **108**, 227–255 (2002).

Souvaliotis, A., and A. N. Beris, "An extended White–Metzner viscoelastic fluid model based on an internal structural parameter," J. Rheol. **36**, 241–271 (1992).

Stoltz, C., J. J. de Pablo, and M. D. Graham, "Concentration dependence of shear and extensional rheology of polymer solutions: Brownian dynamics simulations," J. Rheol. **50**, 137–167 (2006).

Teixeira, R. E., H. P. Babcock, E. S. G. Shaqfeh, and S. Chu, "Shear thinning and tumbling dynamics of single polymer in the flow-gradient plane," Macromolecules **38**, 581–592 (2005).

Teixeira, R. E., A. K. Dambal, D. H. Richter, E. S. G. Shaqfeh, and S. Chu, "The individualistic dynamics of entangled DNA in solution," Macromolecules **40**, 2461–2476 (2007).

Todd, B. D., and P. J. Daivis, "Nonequilibrium molecular dynamics simulations of planar elongational flow with spatially and temporally periodic boundary conditions," Phys. Rev. Lett. **81**, 1118–1121 (1998).

Travis, K. P., P. J. Daivis, and D. J. Evans, "Thermostats for molecular fluids undergoing shear flow: Application to liquid chlorine," J. Chem. Phys. **103**, 10638–10651 (1995).

Tsolou, G., V. G. Mavrantzas, and D. N. Theodorou, "Detailed atomistic molecular dynamics simulation of *cis*-1,4-poly(butadiene)," Macromolecules **38**, 1478–1492 (2005).

Venkataramani, V., R. Sureshkumar, and B. Khomami, "Coarse-grained modeling of macromolecular solutions using a configuration-based approach," J. Rheol. **52**, 1143–1177 (2008).

Williams, G., and D. C. Watts, "Non-symmetrical dielectric relaxation behaviour arising from a simple empirical decay function," Trans. Faraday Soc. **66**, 80–85 (1970).

Williams, G., D. C. Watts, S. B. Dev, and A. M. North, "Further considerations of non symmetrical dielectric relaxation behaviour arising from a simple empirical decay function," Trans. Faraday Soc. **67**, 1323–1335 (1971).